Comparative analysis of opto-electronic performance of aluminium and silver nano-porous and nano-wired layers

Mikita Marus,[1] Aliaksandr Hubarevich,[1] Hong Wang,[1] Andrei Stsiapanau,[2] Aliaksandr Smirnov,[2] Xiao Wei Sun,[1,3] and Weijun Fan[1,*]

[1]*School of Electrical and Electronic Engineering, Nanyang Technological University, 50 Nanyang Avenue, 639798, Singapore*

[2]*Department of Micro- and Nano-Electronics, Belarusian State University of Informatics and Radioelectronics, 6 P. Brovki, Minsk, 220013, Belarus*

[3]*EXWSUN@ntu.edu.sg*

**EWJFAN@ntu.edu.sg*

Abstract: The comparison of optical and electronic properties between squarely and hexagonally arranged nano-porous layers and uniformly arranged nano-wired layers of aluminium and silver was presented. The nano-wired configuration exhibit 20 and 10% higher average transmittance in visible wavelength range in comparison to square and hexagonal nano-porous designs, respectively. The insignificant difference of the transmittance for aluminium and silver nano-porous and nano-wired layers is observed, when interpore/interwire distance is larger than wavelengths of incoming light. This difference becomes considerable at the interpore/interwire distance less than wavelengths of incoming light: silver nano-porous and nano-wired layers possess up to 27% higher transmittance in comparison to aluminium layers.

OCIS codes: (130.0250) Optoelectronics; (310.7005) Transparent conductive coatings; (240.6680) Surface plasmons.

References and links

1. S. Bae, S. J. Kim, D. Shin, J.-H. Ahn, and B. H. Hong, "Towards industrial applications of graphene electrodes," Phys. Scr. **146**, 014024 (2012).
2. D. Zhang, K. Ryu, X. Liu, E. Polikarpov, J. Ly, M. E. Tompson, and C. Zhou, "Transparent, conductive, and flexible carbon nanotube films and their application in organic light-emitting diodes," Nano Lett. **6**(9), 1880–1886 (2006).
3. A. G. MacDiarmid, "Synthetic metals: a novel role for organic polymers," Synth. Met. **40**(14), 11–22 (2001).
4. G. Eda, G. Fanchini, and M. Chhowalla, "Large-area ultrathin films of reduced graphene oxide as a transparent and flexible electronic material," Nat. Nanotechnol. **3**(5), 270–274 (2008).
5. K. S. Kim, Y. Zhao, H. Jang, S. Y. Lee, J. M. Kim, K. S. Kim, J.-H. Ahn, P. Kim, J.-Y. Choi, and B. H. Hong, "Large-scale pattern growth of graphene films for stretchable transparent electrodes," Nature **457**(7230), 706–710 (2009).
6. N. Formica, P. Mantilla-Perez, D. S. Ghosh, D. Janner, T. L. Chen, M. Huang, S. Garner, J. Martorell, and V. Pruneri, "An indium tin oxide-free polymer solar cell on flexible glass," ACS Appl. Mater. Interfaces **7**(8), 4541–4548 (2015).
7. M.-G. Kang and L. J. Guo, "Metal transfer assisted nanolithography on rigid and flexible substrates," J. Vac. Sci. Technol. B **26**(6), 2421–2425 (2008).
8. P. B. Catrysse and S. Fan, "Nanopatterned metallic films for use as transparent conductive electrodes in optoelectronic devices," Nano Lett. **10**(8), 2944–2949 (2010).
9. M. G. Kang, M. S. Kim, J. Kim, and L. J. Guo, "Organic solar cells using nanoimprinted transparent metal electrodes," Adv. Mater. **20**(23), 4408–4413 (2008).
10. M.-G. Kang and L. J. Guo, "Semitransparent Cu electrode on a flexible substrate and its application in organic light emitting diodes," J. Vac. Sci. Technol. B **25**(6), 2637–2641 (2007).
11. J. van de Groep, P. Spinelli, and A. Polman, "Transparent conducting silver nanowire networks," Nano Lett. **12**(6), 3138–3144 (2012).
12. *NanoWeb: sub-micron transparent metal mesh conductors*. Available from: *http://www.rolith.com/applications/transparent-conductive-electrodes*.

#246176 Received 20 Jul 2015; revised 22 Sep 2015; accepted 29 Sep 2015; published 2 Oct 2015

13. L. Martín-Moreno, F. J. García-Vidal, H. J. Lezec, K. M. Pellerin, T. Thio, J. B. Pendry, and T. W. Ebbesen, "Theory of extraordinary optical transmission through subwavelength hole arrays," Phys. Rev. Lett. **86**(6), 1114–1117 (2001).
14. W.-D. Li, J. Hu, and S. Y. Chou, "Extraordinary light transmission through opaque thin metal film with subwavelength holes blocked by metal disks," Opt. Express **19**(21), 21098–21108 (2011).
15. T. W. Ebbesen, H. J. Lezec, H. F. Ghaemi, T. Thio, and P. A. Wolff, "Extraordinary optical transmission through sub-wavelength hole arrays," Nature **391**(6668), 667–669 (1998).
16. J. Bhattacharya, N. Chakravarty, S. Pattnaik, W. D. Slafer, R. Biswas, and V. L. Dala, "A photonic-plasmonic structure for enhancing light absorption in thin film solar cells," Appl. Phys. Lett. **99**(13), 131114 (2011).
17. K. Aydin, V. E. Ferry, R. M. Briggs, and H. A. Atwater, "Broadband polarization-independent resonant light absorption using ultrathin plasmonic super absorbers," Nat. Commun. **2**, 517 (2011).
18. A. Hubarevich, A. Kukhta, H. V. Demir, X. Sun, and H. Wang, "Ultra-thin broadband nanostructured insulator-metal-insulator-metal plasmonic light absorber," Opt. Express **23**(8), 9753–9761 (2015).
19. J. Y. Lee, S. T. Connor, Y. Cui, and P. Peumans, "Solution-processed metal nanowire mesh transparent electrodes," Nano Lett. **8**(2), 689–692 (2008).
20. L. Hu, H. Wu, and Y. Cui, "Metal nanogrids, nanowires, and nanofibers for transparent electrodes," MRS Bull. **36**(10), 760–765 (2011).
21. B. Han, Y. Huang, R. Li, Q. Peng, J. Luo, K. Pei, A. Herczynski, K. Kempa, Z. Ren, and J. Gao, "Bio-inspired networks for optoelectronic applications," Nat. Commun. **5**, 5674 (2014).
22. D. S. Ghosh, L. Martinez, S. Giurgola, P. Vergani, and V. Pruneri, "Widely transparent electrodes based on ultrathin metals," Opt. Lett. **34**(3), 325–327 (2009).
23. M. Marus, A. Hubarevich, H. Wang, A. Smirnov, X. Sun, and W. Fan, "Optoelectronic performance optimization for transparent conductive layers based on randomly arranged silver nanorods," Opt. Express **23**(5), 6209–6214 (2015).
24. A. Hubarevich, M. Marus, W. Fan, A. Smirnov, X. W. Sun, and H. Wang, "Theoretical comparison of optical and electronic properties of uniformly and randomly arranged nano-porous ultra-thin layers," Opt. Express **23**(14), 17860–17865 (2015).
25. *Lumerical FDTD Solutions*. Available from: *https://www.lumerical.com/tcad-products/fdtd/*.
26. B. Last and D. Thouless, "Percolation theory and electrical conductivity," Phys. Rev. Lett. **27**(25), 1719–1721 (1971).
27. J. Fitzpatrick, R. Malt, and F. Spaepen, "Percolation theory and the conductivity of random close packed mixtures of hard spheres," Phys. Lett. A **47**(3), 207–208 (1974).
28. S. Kirkpatrick, "Percolation and conduction," Rev. Mod. Phys. **45**(4), 574–588 (1973).
29. S. Xie, Z. Ouyang, B. Jia, and M. Gu, "Large-size, high-uniformity, random silver nanowire networks as transparent electrodes for crystalline silicon wafer solar cells," Opt. Express **21**(103), A355–A362 (2013).
30. M. Rycenga, C. M. Cobley, J. Zeng, W. Li, C. H. Moran, Q. Zhang, D. Qin, and Y. Xia, "Controlling the synthesis and assembly of silver nanostructures for plasmonic applications," Chem. Rev. **111**(6), 3669–3712 (2011).
31. D. Y. Choi, H. W. Kang, H. J. Sung, and S. S. Kim, "Annealing-free, flexible silver nanowire-polymer composite electrodes via a continuous two-step spray-coating method," Nanoscale **5**(3), 977–983 (2013).
32. H. H. Khaligh and I. A. Goldthorpe, "Failure of silver nanowire transparent electrodes under current flow," Nanoscale Res. Lett. **8**(1), 235 (2013).
33. Q. G. Du, K. Sathiyamoorthy, L. P. Zhang, H. V. Demir, C. H. Kam, and X. W. Sun, "A two-dimensional nanopatterned thin metallic transparent conductor with high transparency from the ultraviolet to the infrared," Appl. Phys. Lett. **101**(18), 181112 (2012).
34. K. Lee, S. H. Song, and J. Ahn, "FDTD simulation of transmittance characteristics of one-dimensional conducting electrodes," Opt. Express **22**(6), 6269–6275 (2014).
35. B. Huttner, "Optical properties of polyvalent metals in the solid and liquid state: aluminium," J. Phys. Condens. Matter **6**(13), 2459–2474 (1994).

1. Introduction

Transparent conductive layers (TCLs) are an inevitable component of various opto-electronic devices: liquid crystal and quantum dot displays, light emitting diodes, solar cells, touch sensors and smart windows [1–5]. Novel opto-electronic devices demand specific properties of TCLs such as flexibility, accessibility, ease of fabrication and low cost [6–10]. Recent studies demonstrate that nanopatterned metallic layers possess all the above mentioned properties, as well as opto-electronic performance exceeding indium-tin-oxide (ITO), which is the most used TCL today [11, 12]. Moreover, surface plasmons, which exist at the interface between metal and dielectric at certain wavelengths, can significantly improve the optical properties of the metallic nanopatterns and/or its surrounding material [13–18]. These facts demonstrate the attractiveness of the nanopatterned metallic layers for the next generation of TCLs.

Two common types of the nano-patterned layers, which are nano-pores (NPs) and nano-wires (NWs), were investigated for being used as TCLs [19–24]. Interpore/interwire distance,

#246176 Received 20 Jul 2015; revised 22 Sep 2015; accepted 29 Sep 2015; published 2 Oct 2015

pore/wire diameter and thickness of the patterned layer can be modified to obtain various application specific transmittance and sheet resistance. For example, the transmittance of 97% and the sheet resistance of 3 Ohm/sq was demonstrated in case of silver NW TCLs [12]. However, it is still unclear which type of the nano-patterned layers can possess better opto-electronic performance. In this paper, the theoretical comparison of the opto-electronic properties between NP layers with square and hexagonal arrangement of the pores and uniformly arranged NW layers for aluminium and silver is demonstrated. We show that NW configuration exhibits higher average transmittance in visible wavelength range than square and hexagonal NP designs.

2. Methodology

Figure 1 shows the geometrical models for NP and NW layers on glass substrate. NPs were arranged squarely (NP_{sq}) and hexagonally (NP_{hex}) with interpore distance *a* and diameter of pore *d* [Figs. 1(a) and 1(b) respectively], while NWs were uniformly arranged with the interwire distance *a* and width of wires *w*. The simulation area was narrowed to the unit cell, which size along *X* and *Y* axes was set to the interpore/interwire distance *a* for the squarely arranged NP and NW layers. In case of the hexagonally arranged NP layers the unit cell was set to *a* and $a \times \sqrt{3}$ along *X* and *Y* axes, respectively.

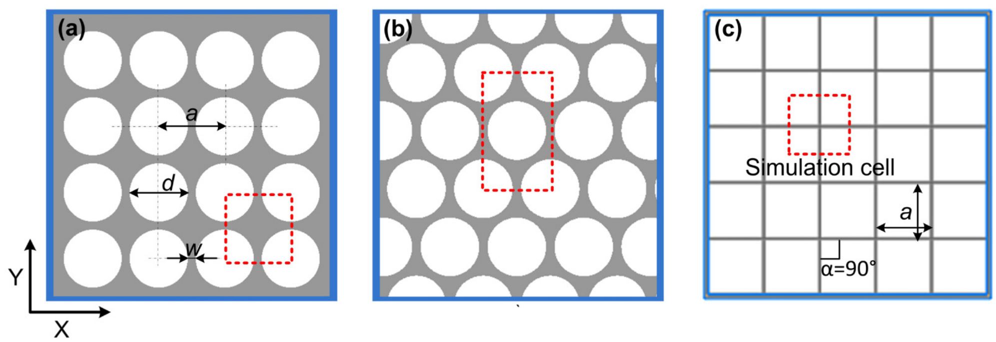

Fig. 1. Geometrical models of the following distributions: squarely (a) and hexagonally (b) arranged NPs with interpore distance *a* and diameter of pores *d*; (c) uniformly arranged NWs with the interwire distance *a* and the width of wires *w*. Red rectangles are the unit simulation cells, which are equal to a^2 for the NPs with square arrangement and NWs and $a^2 \times \sqrt{3}$ for NPs with hexagonal arrangement, respectively.

The optical properties were simulated using the finite-difference time-domain method (FDTD) which is commercially available within Lumerical software [25]. The incident light ranged from 300 to 900 nm was distributed along *Z* axis. The periodic boundary conditions were applied along X and Y axes to simulate a periodic structure in XY plane. While the periodic boundary condition was also applied along Z axis to simulate the “air/layer/glass” structure along Z axis and the perfectly matched layers were applied parallel to XY plane. Mesh size for metallic layer was set to 10, 10 and 5 nm in *X*, *Y*, and *Z* directions, respectively.

The sheet resistance is calculated by percolation model in accordance to [26–28], which is given by the following equation:

$$R_{sh} = \frac{1}{h\sigma_0\left(\phi_f - \phi_{crit}\right)^t}, \tag{1}$$

where σ_0 is the conductivity of metal, ϕ_f is the volume fraction of patterned metal layer, ϕ_{crit} is the volume fraction threshold when the conductivity of patterned metal layer is zero, *h* is the thickness of the metal layer and *t* is the critical exponent. Above mentioned methods were successfully applied by our group in [23, 24].

#246176 Received 20 Jul 2015; revised 22 Sep 2015; accepted 29 Sep 2015; published 2 Oct 2015

3. Results and discussion

The distinction of opto-electronic properties between uniformly and randomly arranged NP layers was previously studied by our group in [24]. It was shown that layers with uniform arrangement of NPs possess higher transmittance (up to 15%) and lower sheet resistance (down to 12 times) compared to random configuration of NPs. Therefore, the randomly arranged NP layers were excluded from the current paper. The thickness of NP and NW layers from 10 to 100 nm is typically implemented within experimental studies [20, 29–34]. We set the height (*h*) of the NWs to 60 nm. The shortest distance between edges of two nearest NPs and the width of NWs, which are equal to the distance *w* in Fig. 1, was set to 60 nm and was kept *fixed* for all simulations, while the interpore/interwire distance *a* was varied from 8 μm to 80 nm. Such interpore/interwire distance was chosen in order to analyze the opto-electronic properties for two regions: interpore/interwire distance less than (i) and larger than (ii) incoming wavelengths. The decrease of *a*, while keeping *w* fixed, results in decrement of open area. For instance, the open areas for NW layers with *a* of 8 μm and 80 nm are equal to 98.51 and 6.25%, respectively. The concentration of NPs and the concentration of NWs were calculated per area of 8×8 μm^2, where the *minimum* amount of NPs (one) and NWs (two: one along *X* and one along *Y* axes) is at $a = 8$ μm and the *maximum* amount of NPs (100) and NWs (200: 100 along *X* and 100 along *Y* axes) is at $a = 80$ nm.

Figure 2 shows the influence of the concentration of NPs (C_{NP}) and concentration of crossings of NWs (C_{NWcrs}) on the transmittance of *Al* NP and NW layers for the wavelength range from 300 to 900 nm. The average transmittance of squarely arranged *Al* NP layers in visible spectrum decreases from 75 to 2.25% when the concentration of NPs increases from 1 to 50, while the hexagonal arrangement of NPs possesses higher average transmittance, which decreases from 85 to 2.5% when C_{NP} increases from 1 to 50. *Al* NW layers *outperform* NP layers and demonstrate the average transmittance ranging from 95 to 5% when C_{NWcrs} increases from 1 to 50. The maximum difference of the transmittance between NP_{sq} and NP_{hex} against NW layers, which is 20 and 10% respectively, is observed at the concentration of NPs and NW_{crs} equal to one. This difference decreases with the increment of concentration of NPs and NW_{crs} and becomes insignificant at $C_{NPs} = C_{NWcrs} = 50$ (less than 2.5%), which is explained by the decrement of open area. Dips of the transmittance in range from 300 to 400 nm are related to localized surface plasmons (LSPs) which are oscillations of electrons inside NP/NW layers along the distance between edges of two pores and in crosswise direction to the individual NWs [11]. Another dip of the transmittance from 700 to 800 nm is due to interband electron transition in *Al* [35]. Continuous decrement in the transmittance from 450 to 850 nm is attributed to surface plasmon polaritons (SPPs), which excite and propagate along the NWs and metal tract between the neighboring rows of NPs [11]. Specific dip of the transmittance is observed only for NP layer in range from 560 to 620 nm, which can be explained by interference between LSPs traveling in opposite directions along the distance between edges of two pores.

Figure 3 shows the influence of the concentration of NPs and concentration of crossings of NWs on the transmittance of *Ag* NP and NW layers for the wavelength range from 300 to

#246176 Received 20 Jul 2015; revised 22 Sep 2015; accepted 29 Sep 2015; published 2 Oct 2015

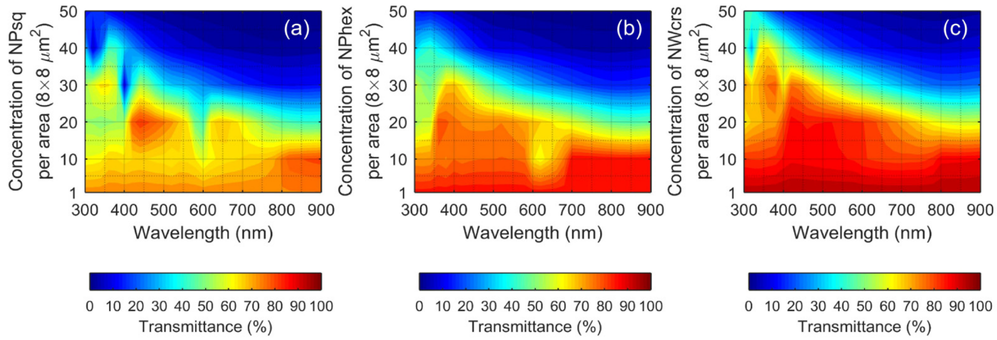

Fig. 2. Dependence of the transmittance of *Al* NP and NW layers on the concentration of NPs with square (a) and hexagonal (b) arrangement and the concentration of crossings of NWs (c) for wavelength range from 300 to 900 nm. Note: one NW_{cr} requires two NWs, two NW_{crs} require four NWs, etc.

900 nm. The average transmittance of squarely arranged *Ag* NP layers in visible spectrum decreases from 75 to 20% when the concentration of NPs increases from 1 to 50, while the hexagonal arrangement of NPs possesses higher average transmittance, which decreases from 86 to 23.2% when C_{NP} increases from 1 to 50. *Ag* NW layers *outperform* NP layers and demonstrate the average transmittance ranging from 95 to 32.7% when C_{NWcrs} increases from 1 to 50. The maximum difference of the transmittance between NP_{sq} and NP_{hex} against NW layers is observed at the concentration of NPs and NW_{crs} equal to one, which is same as in case of *Al* layers (see Fig. 2) and is 20 and 10% respectively. This difference decreases with the increment of concentration of NPs and NW_{crs} and becomes equal to 12.7 and 9.5% between NP_{sq} and NP_{hex} against NW, respectively, which is up to 27% higher in comparison to *Al* layers. This can be explained by higher quality factor of surface plasmons for *Ag* NP/NW layers, which increases the momentum matching between wavevectors of photons and SPPs, resulting in enhanced transmittance. Dips of transmittance for *Ag* NP/NW layers can be explained in the same manner as for *Al* NP/NW layers: (i) dips of the transmittance in range from 300 to 450 nm are related to LSPs; (ii) continuous decrement in the transmittance from 450 to 850 nm is attributed to SPPs; (iii) specific dip of the transmittance in range from 560 to 620 nm related to the interference between LSPs traveling in opposite directions along the distance between edges of two pores. There is no dip of the transmittance from 700 to 800 which is related to interband transition only for *Al*.

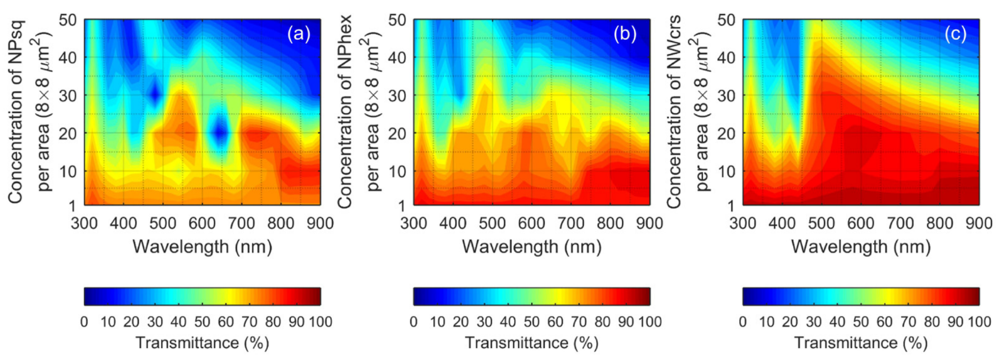

Fig. 3. Dependence of the transmittance of *Ag* NP and NW layers on the concentration of NPs with square (a) and hexagonal (b) arrangement and the concentration of crossings of NWs (c) for wavelength range from 300 to 900 nm. Note: one NW_{cr} requires two NWs, two NW_{crs} require four NWs, etc.

#246176 Received 20 Jul 2015; revised 22 Sep 2015; accepted 29 Sep 2015; published 2 Oct 2015

Figure 4 illustrates the dependence of the sheet resistance against the average transmittance in visible wavelength spectrum for *Al* (left) and *Ag* (right) NP/NW layers. Significant difference between *Al* NP and NW layers becomes evident since the sheet resistance equals to 3 Ohm/sq. In case of *Ag* NP and NW layers this difference takes place at around 1.5 Ohm/sq, which is explained by higher bulk conductivity σ_0 of *Ag*: 6.3×10^7 S/m versus 3.5×10^7 S/m for *Al*. NW layer possesses the transmittance higher by 10 and 20% than NPs layers with hexagonal and square arrangement, respectively. For instance, at the sheet resistance of 5 Ohm/sq the transmittance of NW layer is 90%, while hexagonally and squarely NP layer have the transmittance of only 80 and 70%, respectively. It can be explained by the larger open area of NW layers in comparison with NP arrangement, which results in higher influence of LSPs and SPPs on the transmittance rather than the absorbance and reflectance of NW layers. Interestingly, the values of the transmittance are almost similar for both *Al* and *Ag* at the sheet resistance larger than 20 Ohm/sq. This effect takes place when interpore/interwire distance becomes longer than the wavelength of the incoming light (in our case ≥ 800 nm), resulting in insufficient influence of LSPs and SPPs on the transmittance. Another behavior is observed at the interpore/interwire distance ≤ 800 nm: the transmittance of *Ag* layers is higher by ~20 and ~30% in comparison with *Al* layers for NP and NW, respectively. Thus, metals with higher quality factor of the surface plasmons possess better transmittance for the nanoscale interpore/interwire distance of NP/NW layers.

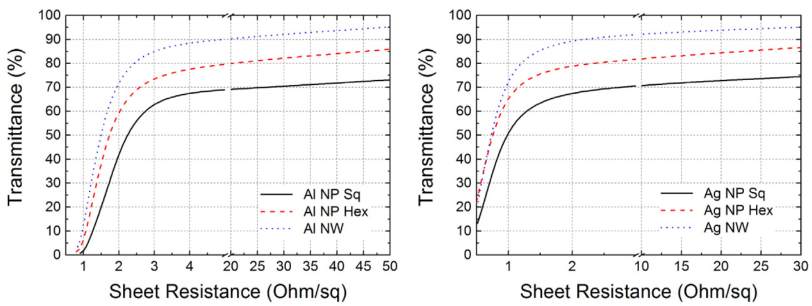

Fig. 4. Sheet resistance versus average transmittance in visible wavelength spectrum for *Al* (left) and *Ag* (right) NPs/NWs layers.

4. Conclusion

The theoretical comparison of the optical and the electronic properties between the squarely and hexagonally arranged NP layers and the uniformly arranged NW layers of *Al* and *Ag* was presented. NW configuration possesses 20 and 10% higher average transmittance in the visible spectrum in comparison to the square and hexagonal NP designs, respectively. The difference of the transmittance for *Al* and *Ag* NP/NW layers is insignificant at the interpore/interwire distance larger than wavelengths of incoming light. This difference becomes considerable at the interpore/interwire distance of subwavelength range, resulting in up to 27% higher transmittance of *Ag* NP/NW layers in comparison to *Al* ones, which is due to the stronger quality factor of the surface plasmons for *Ag*. The given results grant the opportunities for more detailed analysis of the type and material of the nano-patterned transparent conductive layers chosen for different optoelectronic applications, such as displays and solar cells.

Acknowledgment

This project is supported by National Research Foundation of Singapore (No. NRF-CRP11-2012-01).